A.N. MOROZOVSKA,[1] V.V. OBUKHOVSKYI,[2] O.V. UDOD,[3] S.V. KALININ,[4]
O. TSELEV[4]

[1] Institute of Physics, Nat. Acad. of Sci. of Ukraine
   (46, Nauka Ave., Kyiv 03680, Ukraine; e-mail: anna.n.morozovska@gmail.com)
[2] Taras Shevchenko National University of Kyiv, Faculty of Radiophysics
   (4, Academician Glushkov Ave., Kyiv 03022, Ukraine)
[3] I.M. Frantsevych Institute for Problems of Materials Science, Nat. Acad. of Sci. of Ukraine
   (3, Krzhyzhanivskyi Str., Kyiv 03142, Ukraine)
[4] The Center for Nanophase Materials Sciences, Oak Ridge National Laboratory
   (Oak Ridge, TN 37831)

ELECTROMIGRATION AND DIFFUSION RESEARCHES IN SCANNING PROBE MICROSCOPY OF SOLID ELECTROLYTES

The local mechanico-electrochemical response of solid electrolytes has been simulated numerically and analyzed in the Boltzmann–Planck–Nernst–Einstein approximation with regard for the Vegard mechanism. The geometry of the problem is selected to be typical of electrochemical strain microscopy (ESM) experiments. The frequency spectra for various components of the electrolyte surface displacement and the ESM response depth are calculated, as well as the variations of donor concentrations. The corresponding comparative analysis is carried out.

K e y w o r d s: electrochemical strain microscopy, Boltzmann–Planck–Nernst–Einstein approximation, drift-diffusion theory, Vegard's law.

1. Introduction

Strong electromechanical coupling in solid electrolytes, which are used in storage batteries, can be applied to locally detect and visualize processes of lithium deintercalation and diffusion on the nanometer scale. Hence, it allows the mesoscale mechanisms of battery operation to be analyzed in detail. The tip of a scanning probe microscope (SPM) with an applied electric potential operates as a moving electrocatalytic active probe, which examines the local electrochemical activity of the electrolyte near its surface. The probe creates a strongly non-uniform electric field concentrated in a nano-sized volume of the material. The electric field changes the local electrochemical potential of lithium ions on the surface and forces them to intercalate or deintercalate. As a result, the local concentration of moving ions changes owing to the migration (field-induced) and diffusion (concentration-gradient-induced) mechanisms. The distance between certain groups of atoms (the local molar volume) under the tip also varies.

The corresponding changes of the molar volume [1, 2] give rise to local electrochemical deformations owing to a variation in the concentration of ions. The electrochemical deformation of the solid electrolyte surface is measured by SPM at a level of 2–5 pm.

The contact between the tip and the electrolyte can be described by the model of a harmonic oscillator, whose resonance frequency is mainly determined by the Young modulus of this contact region. Using the phase-sensitive detection, the resonance amplitude of the surface displacement measured in nano- or picometer units can be determined with the help of an SPM tip, thus providing information about local variations in the lithium concentration induced by electric potential changes and, hence, about the lithium transport. This method, which was called the electrochemical strain microscopy (ESM) [3–9], is similar to the piezoelectric power microscopy applied to ferroelectric materials and devices [10–12]. The ESM can reveal volume variations corresponding to the total lithiation and delithiation in a monoatomic layer or to the 5–10% variation of lithium concentration in a space interval of 20 nm [3–9]. Electrochemical reactions detected with the help of ESM play an im-

portant role in the operation mechanisms of memristive elements such as the electroforming and the further resistive switching [13, 14]. The localization of an ESM signal at interfaces means that the latter are responsible for the mechanical stability and the irreversible power losses, which points to possible ways to optimize electrolytic substances.

The hysteresis of the surface displacement amplitude as a function of the pulse voltage is observed in ESM if the voltage variation frequency is close to the reciprocal characteristic time of the lithium diffusion [3–9]. Nucleation electric voltages, which are determined from the inflection points in the forward and backward curves [15], do not depend on the tip voltage. Such a behavior reminds rate-independent thermodynamically confined nucleation-like phenomena. The available theoretical models of ESM responses are linear [16–19]. The linear models demonstrate that the correlation between the redistributions of ions and Vegard stresses results in the ESM response in those materials. They correctly describe its frequency spectrum. However, the observed ferroelectric-like hysteresis loops remain mainly uncomprehended. Actually, the thermodynamics of electro-mechanically coupled mixed ionic-electronic solid electrolytes is governed by Vegard stresses and the flexoelectric effect. [17].

One- [18] and two-dimensional [16] analytical models of the linearized diffusion kinetics in the ESM, as well as a two-dimensional analytical model that considers the linearized drift-diffusion kinetics [19], were developed and brought about elliptic loops with a "coercive" voltage. However, the kinetics actually is not such one, since it linearly depends on the applied voltage.

This research is aimed at a self-consistent two-dimensional simulation of a local mechanic-electrochemical response of solid electrolytes, by using the kinetic Boltzmann–Planck–Nernst–Einstein theory. Such a simulation included the simplest kind of nonlinearity inherent to the examined system.

2. Motivation of Researches in the Field of Electrochemical Strain Microscopy

The efficiencies of power supplies and metal-air batteries are considerably confined by the activation of redox reactions [3–6, 20]. Contrary to the recognized role of the reaction kinetics in the processes that run in solid electrolytes at the nano-sized level, their main mechanisms remain unexplained, being described only by macroscopic researches till now. This shortcoming in the fundamental understanding constrains the development of power supplies [3–6, 20].

The detection of electrochemical deformations within the ESM method allows direct measurements to be used, while monitoring the course of reactions on the nanometer scale, i.e. in volumes that are six to eight orders of magnitude smaller than those, while applying the standard electrochemical methods. The nano-sized probing of the electrochemical deformation kinetics opens a wide spectrum of capabilities for researching and testing the mechanisms that are basic for the operation of fuel cells on the basis of solid electrolytes [4].

Strong coupling between the applied voltage and the mechanical stress in a material of power supply electrodes can also be used to measure the local deintercalation distribution and diffusion of lithium on the nanometer scale. Hence, it allows one to study the mechanisms of power supply operation. The visualization of the lithium ion diffusion on separate grains and fixed intergrain boundaries is a first necessary step toward the understanding of the role of extended defects in power losses and a reduction of the power supply capacity. The relevant measurements show that the diffusion ability of lithium ions is higher for certain grains and intergrain boundaries. Hence, the optimization of the ionic conductivity at interfaces between the grains should open a direct way to the enhancement of the electrochemical efficiency of those materials [3].

In the ESM, the tip of a scanning probe microscope with the applied voltage operates as a moving electrocatalyticaly active probe to study the local electrochemical activity. The probe concentrates the electric field in a nano-sized volume of the material, and nano-sized surface displacements caused by the applied potential provide information about local electrochemical processes. This approach allows the activation processes of reactions to be directly visualized. It can be expanded onto a wide spectrum of materials with the oxygen conductivity, as well as electrocatalytic materials [4].

3. Formulation of the Problem

In order to simulate the ESM signal, let us consider the case of mixed ionic-electronic conductivity in an

electrolytic material with moving ionized donors and electrons. The corresponding concentration fields are $N_d^+(\mathbf{r})$ and $n(\mathbf{r})$, respectively. The donors in the material concerned are supposed to be either neutral or singly ionized. The neutral donors are fixed, whereas the charged ones can move [21]. The geometry of the problem used in calculations is illustrated in Fig. 1.

Owing to the axial symmetry of the contact between the probe tip and the surface, the mathematical formulation of the problem becomes simpler in cylindrical coordinates. The electric potential $\varphi(\mathbf{r})$ under the tip can be calculated self-consistently in the quasistatic approximation, as a solution of the boundary problem

$$\left(\frac{\partial^2}{\partial z^2} + \frac{1}{\rho}\frac{\partial}{\partial \rho}\left(\rho\frac{\partial}{\partial\rho}\right)\right)\varphi(\mathbf{r}) =$$
$$= -\frac{q}{\varepsilon_0\varepsilon}\left(N_d^+(\mathbf{r}) - n(\mathbf{r})\right), \tag{1a}$$

$$\varphi(\rho, z = \sqrt{R_0^2 - \rho^2}, t) = V_0(t),$$
$$\frac{\partial\varphi}{\partial z}(\rho > 0, z = 0, t) = 0, \quad \varphi(\rho, z = h) = 0, \tag{1b}$$

where $\mathbf{r} = \{x, y, z\}$ is the radius vector, $\rho = \sqrt{x^2 + y^2}$ is the radius in the polar coordinate system, $q = 1.6 \times 10^{-19}$ C is the elementary charge, $\varepsilon_0 = 8.854 \times 10^{-12}$ F/m is the electric permittivity of vacuum, ε the relative dielectric permittivity of the electrolyte, h the electrolyte thickness, and R_0 the radius of the probe tip at its contact with the electrolyte surface. The boundary conditions correspond to the case of ESM experiments without the conducting water meniscus [22,23], which is formed at the contact of the probe tip with the surface in the case of increased humidity of air around the tip and the hydrophilic contact. A difference between those cases consists in that, for the ideal tip-surface contact, the contact radius amounts to 3–10 nm and can be determined, by using the classical theory of contact interaction, and the mechanical stresses are determined over the whole contact region. In the case of a water droplet, the region of electric contact is much larger (0.1–1 μm), and the stresses are determined only over the area of mechanical contact between the tip and the surface.

For a small periodic electric potential $V_0(t) \approx V_0\exp(i\omega t)$, it is supposed that the periodic variations of $N_d^+(\mathbf{r}, t)$ and $n(\mathbf{r}, t)$ are induced by the periodic electric potential of the contact, $\varphi(\mathbf{r}, t)$; however, the steric limit is not achieved, and the Boltzmann–Planck–Nernst–Einstein approximation can be ap-
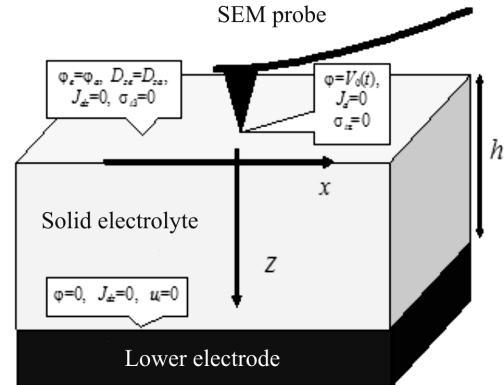

Fig. 1. Typical geometry of the electrochemical strain microscopy. The boundary conditions are indicated

plied to the currents and the electric potential. Therefore, a linear drift-diffusion model is used for the ionic and electron currents:

$$J_d \approx D_d\nabla N_d^+ - \eta_d N_d^+\nabla\varphi, \tag{2a}$$
$$J_n \approx D_n\nabla n - \eta_d n\nabla\varphi. \tag{2b}$$

Further, it is supposed that the diffusion, $D_{d,n}$, and mobility, $\eta_{n,d}$, coefficients are constant [24,25]. Then, the Planck–Nernst–Einstein kinetic equations [26,27] look like

$$\frac{\partial N_d^+}{\partial t} + \frac{1}{q}\mathrm{div}\,\mathbf{J}_d = 0, \tag{3a}$$
$$-\frac{\partial n}{\partial t} + \frac{1}{q}\mathrm{div}\,\mathbf{J}_n = 0. \tag{3b}$$

On the right-hand sides of Eqs. (3), the terms corresponding to ionization and recombination are neglected, assuming that the local equilibrium is maintained, and the mobility of ionized donors is high enough. Those terms have to be taken into account if the donors are fixed.

The boundary conditions for the kinetic equations (3) are as follows: the tip-surface interface is considered to be impenetrable for donor ions and, consequently, there are no ionic currents through the interface:

$$J_{dz}(\rho, z = 0, t) = 0, \quad J_{dz}(\rho, z = h, t) \to 0. \tag{4a}$$

Since we assume that the lateral surfaces of the specimen are located in a dielectric environment, circular currents are absent. Therefore,

$$\mathbf{J}_d(\rho \to \infty, t) = 0, \quad \mathbf{J}_n(\rho \to \infty, t) = 0. \tag{4b}$$

Parameter	Range of possible values	Values used for illustration
Contact radius of the probe R_0	1–1000 nm	5 nm
Relative dielectric permittivity ε	1–100	10
Film thickness h	10 nm–100 μm	150 nm
Applied voltage amplitude V_0	0.01–10 V	1 V
Voltage oscillation frequency ω	1 Hz–1 MHz	300 kHz, period 0.333×10^{-6} s
Concentrations $\bar{N}_d^+$ and $\bar{n}$	10^{23}–10^{26} m^{-3}	1.661 mol/m^3 ($\equiv 10^{24}$ m^{-3})
Donor diffusion coefficient D_d	10^{-16}–10^{-12} m^2/s	10^{-14} m^2/s
Electron diffusion coefficient D_n	$D_n \propto (10$–$10^3)D_d$	10^{-12} m^2/s
Mobilities $\eta_{n,d}$	$\eta_n = qD_n/k_{\mathrm{B}}T$	4.0091×10^{-16} s·mol/kg
	$\eta_d = qD_d/k_{\mathrm{B}}T$	4.0091×10^{-18} s·mol/kg
Coefficients in Chang–Yaffe equation $w_{0,1}$	0, in the case $J_{nz}(\rho,0) = J_{nz}(\rho,h) = 0$	
	∞, in the case $n(\rho,0,t) = n(\rho,h,t) = n_0$	10^{-3} m/s
Concentration n_0	10^{27}–10^{29} m^{-3}	10^{24} m^{-3}
Poisson's ratio ν	0.25–3	0.25
Vergard tensor β_{ij}	0.1–0.01 m^3/mol	
	for simplification, $\beta_{11} = \beta_{33}$	0.1 m^3/mol
Density	$(1$–$3) \times 10^3$ kg/m^3	2×10^3 kg/m^3

The boundary conditions for the electron current are taken in the Chang–Jaffe linearized form [28]:

$$J_{nz}(\rho, z = 0) = w_0\,(n(\rho, z = 0, t) - n_0),$$
$$J_{nz}(\rho, z = h) = w_1\,(n(\rho, z = h, t) - n_1). \qquad (4c)$$

The constants $w_{0,1}$ are the positive quantities related to the surface recombination rate of electrons and holes, respectively [29]. Their specific numerical values are determined by materials of the electrode and the studied specimen. If they are infinitely large, the equilibrium concentration of electrons at the contacts are determined by the electrodes and do not depend on the applied voltage [30]. Therefore, condition (4c) contains a continuous transition from an "open" ohmic contact ($w \to \infty \Rightarrow \delta n(\rho, 0, t) = 0$) to an interface with a confined kinetics ($w > 0$) and to a completely "blocking" contact ($w = 0$).

For the specific case where the chemical contribution is a dominating mechanism for the emergence of a mechanical stress, the generalized Hooke law for a chemically active solid elastic medium includes stresses caused by a variation of the ionic concentration $\delta N_d^+(\mathbf{r}, t) = \left(N_d^+(\mathbf{r}, t) - \bar{N}_d^+\right)$, the mechanical stress tensor σ_{ij}, and the elastic strain u_{ij} [2, 16]:

$$u_{ij}(\mathbf{r}, t) = \beta_{ij}\,\delta N_d^+(\mathbf{r}, t) + s_{ijkl}\sigma_{kl}(\mathbf{r}, t), \qquad (5)$$

where s_{ijkl} is the elastic compliance tensor, and β_{ij} the Vegard tensor, which is also known as the elastic dipole.

As a rule, the size of a contact region in the ESM experiment is considerably smaller than one micron. The corresponding characteristic resonance frequencies of the material are in the GHz range, which is much higher than practically important restrictions imposed on both the dynamics of ions and the ESM-based detection of localized mechanical vibrations. This fact allows the quasistatic approximation to be applied to mechanical phenomena. The general equation of mechanical equilibrium, $\partial \sigma_{ij}/\partial \sigma_{ij}\partial x_j = 0$, was solved in the quasistatic case. This equation gives rise to an equation for the vector of mechanical displacement u_i in the main part of the system,

$$c_{ijkl}\frac{\partial^2 u_k}{\partial x_j \partial x_l} - c_{ijkl}\,\beta_{kl}\,\frac{\partial \delta N_d^+}{\partial x_j} = 0. \qquad (6a)$$

The boundary conditions at the free surface look like

$$\left(c_{ijkl}\frac{\partial u_k}{\partial x_l} - c_{ijkk}\,\beta_{kl}\,\delta N_d^+\right)n_j\bigg|_{z=0} = 0, \qquad (6b)$$

where c_{ijkl} is the mechanical rigidity tensor, and n_j are the components of a normal to the surface.

Below, we will confine the consideration to the transversely isotropic Vegard tensor, $\beta_{ij} = \delta_{ij}\beta_{ii}$,
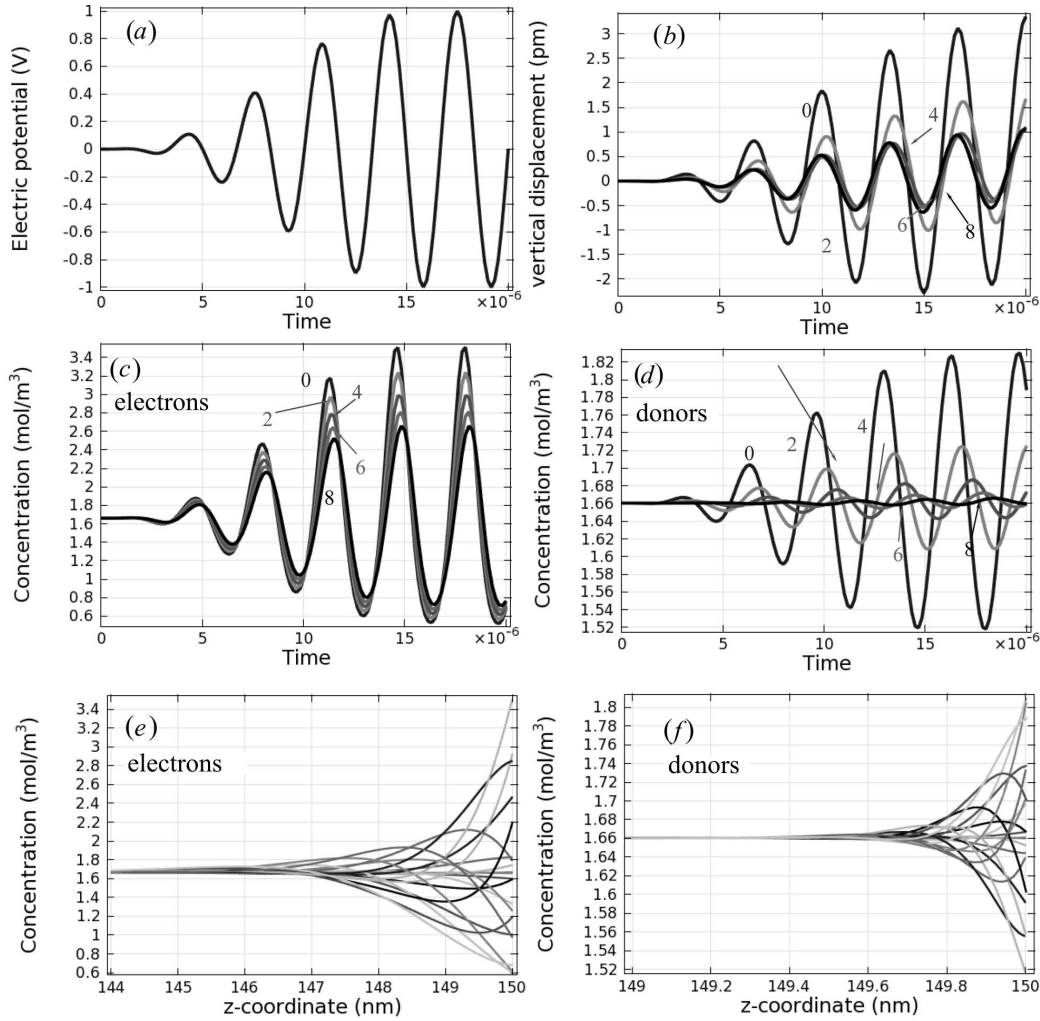
1030

Fig. 2. Time dependences of the applied voltage (a), vertical displacement of the electrolyte (b), and electron (c) and donor (d) concentrations calculated at various distances from the surface $z = 0$, 2, 4, 6, and 8 Å (indicated by numbers near the curves) along the probe axis ($\rho = 0$). Distributions of electrons (e) and donors (f) near the tip-surface contact ($\rho = 0$) at various time moments (various curves with a time step of 10^{-6} s). The diffusion coefficient ratio $D_n/D_d = 10^3$

with $\beta_{11} = \beta_{22} \neq \beta_{33}$. The spectrum of surface displacements at the tip-surface contact ($z = 0$), which is induced by the redistribution of moving donors and can be measured by the SPM electronics, is determined in the case of elastic-homogeneous half-space by the formula [31]

$$u_3(\rho, 0, \omega) = \int\limits_0^\infty dk J_0(k\rho)k \int\limits_0^\infty dz \big(\beta_{33}(1 + k\,z) +$$

$$+ \beta_{11}(1 + 2\nu - k\,z)\big)\exp(-k\,z)\delta\tilde{N}_d^+(k, z, \omega). \quad (7)$$

Here, ν is Poisson's ratio, $k^2 = k_x^2 + k_y^2$, $\delta\tilde{N}_d^+(k, z, \omega)$ is the two-dimensional Fourier transform and the fre-

quency spectrum of the deviation field of the ion concentration $\delta N_d^+(\mathbf{r}, t)$, and $J_0(x)$ is the Bessel function of the zero order. The boundary conditions $\sigma_{3j}(z = 0, t) = 0$ correspond to a mechanically free surface at $z = 0$.

4. Self-Consistent Simulation of an ESM Local Response in Solid Electrolytes with regard for First-Order Nonlinear Effects

The numerical solution of the system of equations (1)–(6) was carried out with the help of the software package COMSOL Multiphysics for the param-
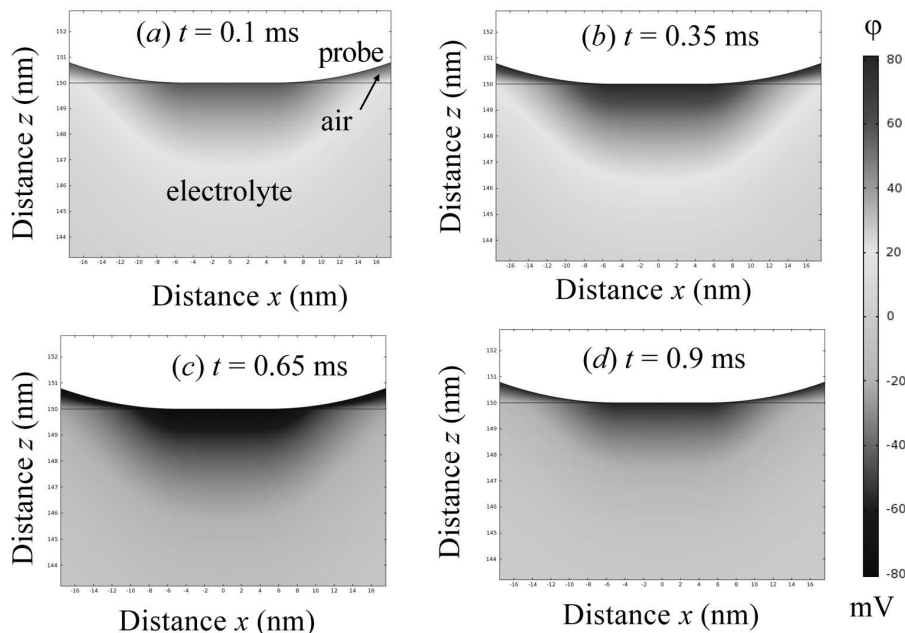
Fig. 3. Distribution maps in the (x, z)-coordinates for the electric potential φ near the ESM probe calculated for various time moments $t = 0.1$ (a), 0.35 (b), 0.65 (c), and 0.9 ms (d). The period of applied alternating voltage is 1 ms

eters quoted in Table. A potential periodic in time, $V_0(t) \propto \sin(\omega t)$, and modulated by a smooth function similar to tanh in order to minimize the excitation of vibrations of the system during the simulation was applied to the probe. The transient process is supposed to terminate, and Figs. 3 to 6 illustrate only steady-state vibrations in the case of ion- and electron-blocking electrodes.

The results of numerical simulation are depicted in Fig. 2. The applied voltage $V_0(t)$ modulated by a tanh-shaped function is shown in Fig. 2, a. It is worth emphasizing that the electric potential $\varphi(t)$ is almost identical to $V_0(t)$ in a thin layer under the electrolyte surface. However, the vertical mechanical displacement of the electrolyte (actually, this is an ESM signal) and the concentration of donors tend rather quickly to the corresponding bulk values within the limits of this layer (see Figs. 2, b and c). A comparison of Fig. 2, c and d shows that electrons and donors oscillate in antiphase, whereas the oscillations of the donor concentration are cophased with the vertical displacement (but in antiphase with the applied voltage). The difference between the penetration depths of electron and donor concentration waves is determined by the difference between the electron and

donor diffusion coefficients, which are related, in turn, to the corresponding diffusion lengths proportional to $\sqrt{\omega D_i}$ (cf. Figs. 2, e and f).

In Fig. 3, the distribution of the electric potential under the ESM probe at various time moments within a period of the applied voltage is shown. At the initial moment, the value of electric potential under the probe equals 60 mV (Fig. 3, a). After a quarter period, the maximum value of the potential reaches 80 mV (Fig. 3, b). During the next 0.3 ms, the electric potential under the probe decreases to -80 mV (Fig. 3, c). At the end of the period, the potential grows to -60 mV (Fig. 3, d).

In Fig. 4, the distribution of the electron concentration at various time moments within a period of the applied voltage is shown. At the initial moment, the electron concentration under the ESM probe equals 2 mol/m^3 (Fig. 4, a). Then it grows by 10% as a result of the electric potential increase (Fig. 4, b). When the potential decreases, the electron concentration near the probe falls down to 1.26 mol/m^3 (Fig. 4, c). At the end of the applied voltage period, the electron concentration starts to grow to 1.33 mol/m^3 (Fig. 4, d).

The distribution of the ion concentration near the ESM probe at various time moments is depicted in
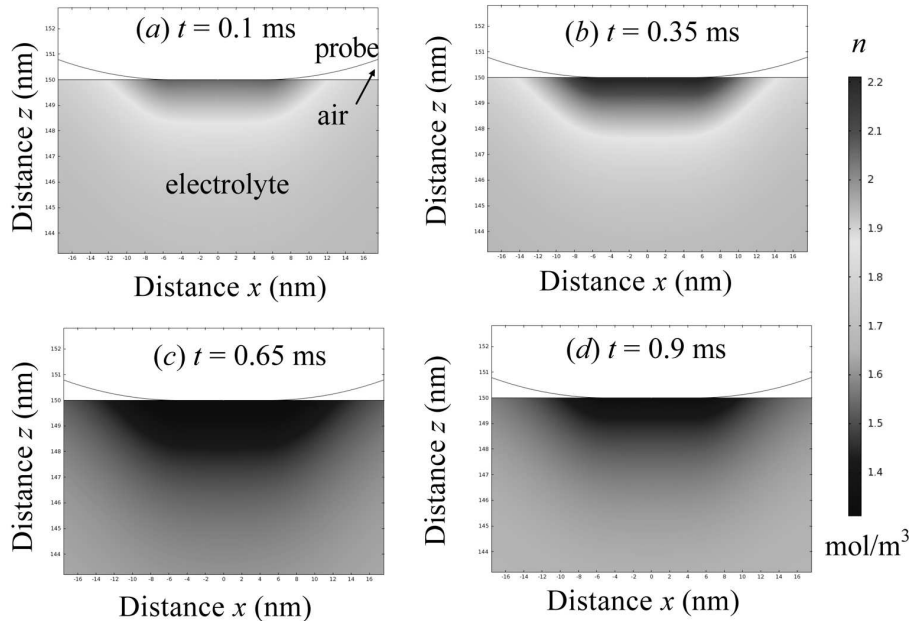
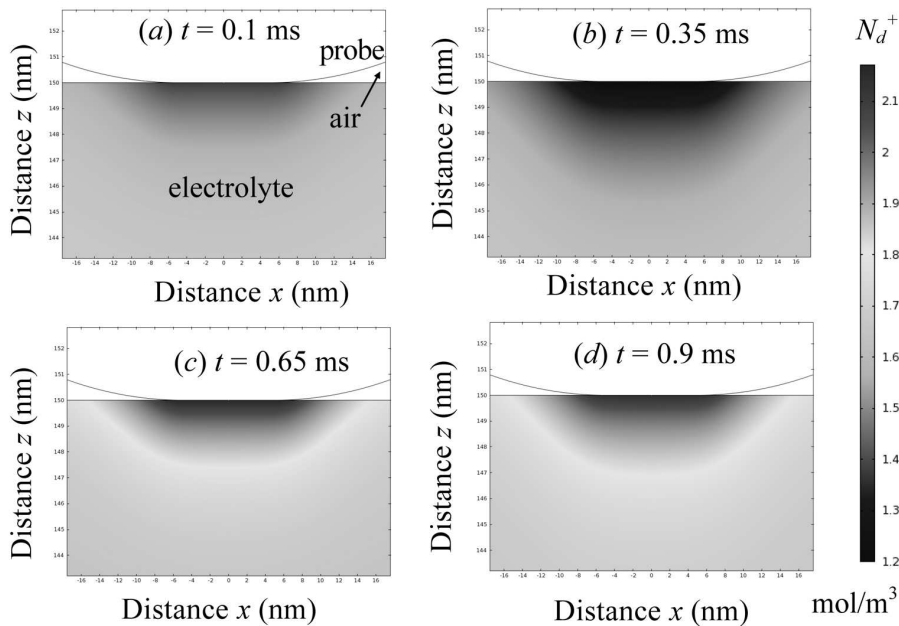**Fig. 4.** The same as in Fig. 3, but for the electron concentration n

Fig. 5. The same as in Fig. 3, but for the ion concentration N_d^+

Fig. 5. At first, the maximum concentration of ions under the probe equals 1.38 mol/m^3 (Fig. 5, a). During the first part of the period, it decreases by 15% (Fig. 5, b); then it increases to 2.17 mol/m^3, when the electric potential decreases (Fig. 5, c). At the last

moment, the ion concentration near the probe falls down to 2.14 mol/m^3 (Fig. 5, d).

The evolution of the distribution of the vertical displacement $u_3(\rho, z)$ near the ESM probe is illustrated in Fig. 6. At the initial time moment, the ver-
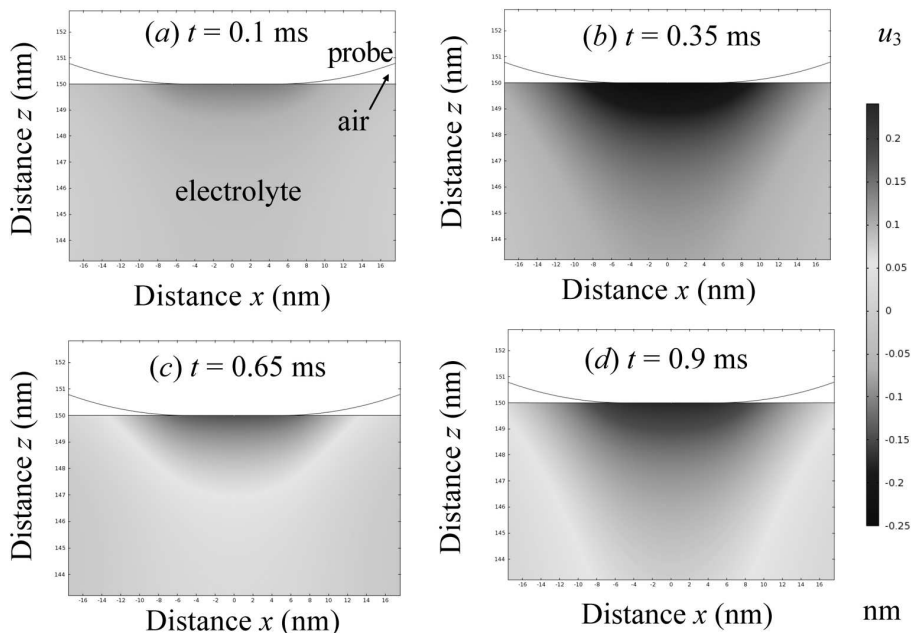
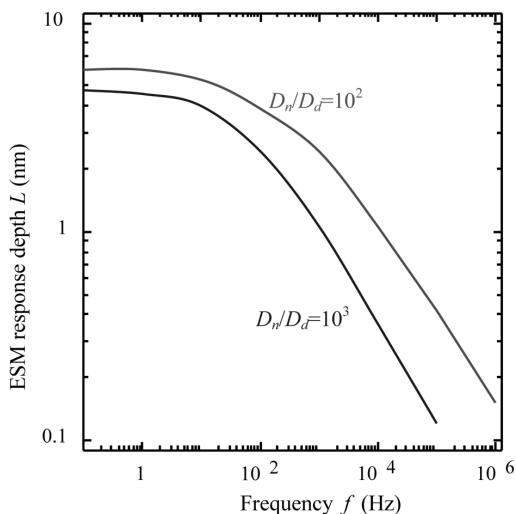**Fig. 6.** The same as in Fig. 3, but for the vertical displacement u_3

Fig. 7. Dependences of the ESM response depth on the applied voltage frequency f for ratios $D_n/D_d = 10^2$ and 10^4. The diffusion coefficient for electrons equals $D_n = 10^{-12}$, and the voltage amplitude is 10 mV

tical displacement under the probe equals -0.11 nm (Fig. 6, a). Then, it decreases further to -0.25 nm due to the reduction of the ion concentration by 15% (Fig. 6, b). Afterward, it grows to 0.18 nm following the ion concentration growth to 2.17 mol/m^3

(Fig. 6, c). At the end of the period, the vertical displacement grows by 33% and ultimately equals 0 24 nm, which corresponds to an ion concentration of 2.14 mol/m^3 (Fig. 6, d). While calculating the potential and the motion of free carriers, this small displacement of the surface – it is at least an order of magnitude smaller than the thickness of the layer, in which carriers undergo a substantial influence of the probe field – was not taken into account.

We also analyzed the properties of the ESM response depth as a function of the frequency f of the alternating voltage and the variation of the donor diffusion coefficient D_d. Typical results are exhibited in Fig. 7 for frequencies of 0.1 Hz–1 MHz. At frequencies lower than 10 Hz, the numerical convergence was obtained, only when the voltage amplitude V_0 was reduced (by the way, this result agrees with the divergence in the static limit predicted theoretically in work [19]). The frequency spectra of the ESM response depth L obey the law $L(f) \propto 1/\sqrt{f}$ at high frequencies, irrespective of the ratio D_n/D_d. As was expected, the low-frequency static limit u_3 does not depend on the transport characteristics such as the diffusion coefficients and their ratio. The static limit u_3 is determined by the change of the total electric charge of ions [17].

5. Conclusions

An additional module to the software package Comsol Multiphysics has been developed and used to self-consistently simulate the SPM local response (the local displacement of the electrolyte surface) in solid electrolytes with regard for nonlinear effects, by using the Boltzmann–Planck–Nernst–Einstein approximation and the Vegard mechanism. Vegard deformations caused by the migration of ions are shown to really stimulate the elastic displacement of the electrolyte surface, which can be directly measured by the SPM. It is demonstrated that the frequency spectrum of both vertical displacement and response depth is saturated at low frequencies of the electric field applied to the SPM probe and satisfies a power law at high ones. It is shown that the SPM local response is not proportional to the average deviation of the donor concentration. In the case of low electric fields, there is a constant phase shift between the SPM response and the voltage applied to the probe. The results of the nonlinear theory agree well with those obtained in the specific case of low electric fields in the framework of the linear drift-diffusion theory.

1. S.R. Bishop, K.L. Duncan, and E.D. Wachsman, Electrochim. Acta **54**, 1436 (2009).
2. G.G. Botte, V.R. Subramanian, and R.E. White, Electrochim. Acta **45**, 2595 (2000).
3. N. Balke, S. Jesse, A.N. Morozovska, E. Eliseev, D.W. Chung, Y. Kim, L. Adamczyk, R.E. Garcıa, N. Dudney, and S.V. Kalinin, Nature Nanotechn. **5**, 749 (2010).
4. A. Kumar, F. Ciucci, A.N. Morozovska, S. Kalinin, and S. Jesse, Nature Chem. **3**, 707 (2011).
5. S. Jesse, N. Balke, E. Eliseev, A. Tselev, N.J. Dudney, A.N. Morozovska, and S.V. Kalinin, ACS Nano **5**, 9682 (2011).
6. N. Balke, E.A. Eliseev, S. Jesse, S. Kalnaus, C. Daniel, N.J. Dudney, A.N. Morozovska, and S.V. Kalinin, J. Appl. Phys. **112**, 052020 (2012).
7. A. Kumar, M.T. Arruda, Y. Kim, I.N. Ivanov, S. Jesse, C.W. Bark, N.C. Bristowe, E. Artacho, P.B. Littlewood, C.-B. Eom, and S.V. Kalinin, ACS Nano. **6**, 3841 (2012).
8. N. Balke, S. Jesse, Y. Kim, L. Adamczyk, I.N. Ivanov, N.J. Dudney, and S.V. Kalinin, ACS Nano **4**, 7349 (2010).
9. N. Balke, S. Jesse, Y. Kim, L. Adamczyk, A. Tselev, I.N. Ivanov, N.J. Dudney, and S.V. Kalinin, Nano Lett. **10**, 3420 (2010).
10. A. Gruverman and A. Kholkin, Rep. Prog. Phys. **69**, 2443 (2006).
11. S.V. Kalinin, A.N. Morozovska, L.Q. Chen, and B.J. Rodriguez, Rep. Prog. Phys. **73**, 056502 (2010).
12. A. Kumar, O.S. Ovchinnikov, H. Funakubo, S. Jesse, and S.V. Kalinin, Appl. Phys. Lett. **98**, 202903 (2011).
13. D.B. Strukov, G.S. Snider, D.R. Stewart, and R.S. Williams, Nature **453**, 80 (2008).
14. K. Szot, W. Speier, G. Bihlmayer, and R. Waser, Nat. Mater. **5**, 312 (2006).
15. S. Jesse, H.N. Lee, and S.V. Kalinin, Rev. Sci. Instrum. **77**, 073702 (2006).
16. A.N. Morozovska, E.A. Eliseev, N. Balke, and S.V. Kalinin, J. Appl. Phys. **108**, 053712 (2010).
17. A.N. Morozovska, E.A. Eliseev, A.K. Tagantsev, S.L. Bravina, Long-Qing Chen, and S.V. Kalinin, Phys. Rev. B **83**, 195313 (2011).
18. A.N. Morozovska, E.A. Eliseev, S.V. Kalinin, Appl. Phys. Lett. **96**, 222906 (2010).
19. A.N. Morozovska, E.A. Eliseev, S.L. Bravina, F. Ciucci, G.S. Svechnikov, Long-Qing Chen, and S.V. Kalinin, J. Appl. Phys. **111**, 014107 (2012).
20. N. Balke, S. Jesse, Y. Kim, L. Adamczyk, I.N. Ivanov, N.J. Dudney, and S.V. Kalinin, ACS Nano **4**, 7349 (2010).
21. Y. Gil, O.M. Umurhan, and I. Riess, J. Appl. Phys. **104**, 084504 (2008).
22. M. Molotskii, J. Appl. Phys. **97**, 014109 (2005).
23. B.L. Weeks, M.W. Vaughn, and J.J. DeYoreo, Langmuir **21**, 8096 (2005).
24. J.R. Macdonald, J. Chem. Phys. **58**, 4982 (1973).
25. I. Riess and J. Maier, Phys. Rev. Lett. **100**, 205901 (2008).
26. J. Jamnik and J. Maier, J. Electrochem. Soc. **146**, 4183 (1999).
27. Zhan Chen, J. Electrochem. Soc. **151**, A1576 (2004).
28. H.-Ch. Chang and G. Jaffe, J. Chem. Phys. **20**, 1071 (1952).
29. G. Nanz, in *Simulation of Semiconductor Devices and Processes, Vol. 4*, edited by W. Fichiner and D. Aemmer (Hartung-Gorre, Zurich, 1991), p. 321.
30. Y. Gil, O.M. Umurhan, and I. Riess, Solid State Ionics **178**, 1 (2007).
31. A.N. Morozovska, E.A. Eliseev, and S.V. Kalinin, J. Appl. Phys. **111**, 014114 (2012).

Г.М. Морозовська, В.В. Обуховський,
О.В. Удод, С.В. Калінін, О. Целев

ДОСЛІДЖЕННЯ ЕЛЕКТРОМІГРАЦІЇ ТА ДИФУЗІЇ В СКАНУЮЧІЙ ЗОНДОВІЙ МІКРОСКОПІЇ ТВЕРДИХ ЕЛЕКТРОЛІТІВ

Р е з ю м е

Проведено чисельне моделювання та аналіз локального механо-електро-хімічного відгуку твердих електролітів в наближенні Больцмана–Планка–Нернста–Ейнштейна з урахуванням вегардівського механізму. Розрахована геометрія є типовою для експериментів у галузі скануючої зондової мікроскопії електрохімічних деформацій (СЗМЕД). Розраховано частотні спектри різних компонент зміщення поверхні електроліту та глибини відгуку СЗМЕД, а також зміни концентрацій донорів, і проведено їх порівняльний аналіз.